Journal of the European Ceramic Society 20 (2000) 569–582

Hexaluminates as a cleavable fiber–matrix interphase: synthesis, texture development, and phase compatibility☆

Michael K. Cinibulk*

Air Force Research Laboratory, Materials and Manufacturing Directorate, Wright-Patterson Air Force Base, OH 45433-7817, USA

Accepted 13 August 1999

Abstract

The current state of research on hexaluminates as a potential cleavable oxide fiber–matrix interphase is reviewed. Calcium hexaluminate was used initially to produce highly textured fiber coatings and interphases in single-crystal alumina fiber-based ceramic–matrix composites. Cracks were shown to deflect and propagate within the interphase by cleavage. Critical strain-energy release rates of 2.2 J/m^2 were measured for highly textured polycrystalline $CaAl_{12}O_{19}$ interphases. Subsequent work has focused on lowering the temperature for synthesis and texturing of both calcium- and lanthanum-based hexaluminates. Doping of hexaluminates, primarily with transition-metal oxides, allows for their formation at temperatures as low as 1000°C. Grain-growth rates are about an order of magnitude greater than for undoped powders. Textured coatings have been grown on single-crystal YAG plates at 1200°C. However, there does not seem to be an adequate driving force for grain growth and texturing of the coatings on polycrystalline alumina fibers (Nextel™ 610) at 1200°C, the maximum processing temperature for these fibers. The lack of a more refractory, commercially available fiber that is phase compatible with the hexaluminates currently limits further development of a hexaluminate fiber–matrix interphase.

Keywords: Aluminosilicate fibers; $CaAl_{12}O_{19}$; Coatings; Grain growth; Interfaces; Mechanical properties; YAG

1. Introduction

Nonoxide fiber-reinforced ceramic–matrix composites (CMCs) typically contain a layer of carbon or hexagonal boron nitride at the fiber–matrix interface to encourage matrix cracks to deflect away from the fiber. Graphite and BN have essentially perfect cleavage, in that they fracture readily along the basal (0001) plane. However, it is not clear whether crack deflection in these composites is solely the result of cleavage of grains within the interphase or debonding due to a weak fiber-coating interface. For example, carbon interphases in tough CMCs with graphitic basal planes parallel to the interface,[1] very weakly textured parallel to the interface,[2,3] graphitic coatings with no texture,[4] porous turbostratic carbon,[5] amorphous carbon,[1,6–9] and multilayered coatings with textured graphitic, untextured graphitic, and amorphous carbon layers[1] have all been reported. Turbostratic hexagonal BN was reported to perform better than fully crystallized hexagonal BN,[10] but in another study cracks deflected very near the BN–glass interface where turbostratic BN was better aligned with the interface.[11] These seemingly contradictory results make it difficult to rely on carbon or BN as models when designing alternate crack-deflecting interphases based on cleavage. However, obvious parameters to consider include fracture-energy anisotropy, degree of texture of cleavage planes, and coating thickness.

An analogue to graphite or BN is needed that is stable in oxidizing conditions at elevated temperatures. A material, with a sufficiently high anisotropy in fracture energy, for crack deflection to occur within the interlayer, is necessary. The criterion usually employed to specify a suitable candidate is that fracture-energy release-rate anisotropy must be at least a factor of four,[12] and the coating must be textured so that cleavage planes are parallel to the interface. However, the required degree of texture that is necessary to deflect and contain the crack is unknown. Nevertheless, if an interlayer material with poor cleavage is substituted for one with perfect cleavage, it seems to follow that either better texture or a thicker coating may be required.

☆ Supported by the Air Force Research Laboratory under Contract No. F33615-96-C-5258.

* Present address: UES Inc., Dayton, OH 45432-1894, USA.

0955-2219/00/$ - see front matter
PII: S0955-2219(99)00255-1

Besides fracture anisotropy and texture, intrinsic high-temperature stability in air and thermochemical stability with potential CMC fiber and matrix phases is needed.

Oxides that have been investigated include the micas, hexaluminates, and some layered perovskites. Evidence for crack deflection at room temperature was found in laminates with mica interphases.[13–15] However, micas dehydrate and decompose to alumina, feldspars or feldspathoids, and/or other oxides at 500–900°C.[13] Fluoromicas such as potassium-fluorophlogopite [$KMg_3(AlSi_3)O_{10}F_2$] are stable above 1200°C in a dry or closed environment at ambient pressure.[13] However, in an open environment with water vapor, potassium-fluorophlogopite starts to breakdown to forsterite, potassium-aluminosilicates, and HF at 1000°C.[13] Similarly, oxides with sufficiently good cleavage to be lubricious, such as talc ($Mg_3Si_4O_{12}H_2$) and pyrophyllite ($Al_2Si_4O_{12}H_2$) are well known. Unfortunately, all are hydrous and decompose at temperatures of interest for CMCs.[16]

Layered perovskites, such as $KCa_2Nb_3O_{10}$, were investigated for suitable crack deflection behavior and were found to have some potential for this application.[17] $KCa_2Nb_3O_{10}$ is reportedly stable up to 1500°C with respect to melting or incongruent vaporization of alkali oxide, and is compatible with alumina to at least 1200°C, but is not compatible with silica. Recent work[17] suggests that interlayers texture properly and are capable of crack deflection. However, they are chemically complex and as such are compatible with a very limited number of potential CMC constituent phases.

A review of the work on hexaluminates, primarily calcium hexaluminate ($CaAl_{12}O_{19}$, the mineral hibonite) and lanthanum hexaluminate ($LaAl_{11}O_{18}$) synthesis and fiber coatings for CMCs is the focus of this paper.

2. Structure and chemistry of the hexaluminates

Hexagonal aluminates, having the β-alumina or magnetoplumbite structures, are commonly referred to as hexaluminates;[18] both structures are composed of layered spinel blocks $[Al_{11}O_{16}]^+$ separated by mirror planes $[M^+O]^-$ and $[M^{2+}AlO_3]^-$, respectively, in which the stabilizing cations (M^+ or M^{2+}) reside (Fig. 1). The structure that is preferred depends on the radius and valence of the stabilizing cation. In general, the alkali oxides react with alumina to form β-aluminas, while alkaline-earth and rare-earth oxides form magnetoplumbites. The mineral magnetoplumbite, $Pb(Fe, Mn, Al)_{12}O_{19}$, is prototypical of a larger class of compounds with the general composition $A^{2+}B^{3+}_{12}O_{19}$.[19] The isostructural hexaluminates are formed by replacing Fe^{3+} with Al^{3+}, and Pb^{2+} with either alkaline-earth or rare-earth cations of similar radii. Only when Pb^{2+} is replaced by Ca^{2+} or Sr^{2+} is the stoichiometric composition obtained. When Pb^{2+} is replaced by a trivalent lanthanide cation a nonstoichiometric, highly defective structure is produced.[20] The ideal structure of $LaAl_{11}O_{18}$ can be represented as $LaO_2[Al_{11}O_{16}]$. By substituting a divalent cation for one Al^{3+} local charge balance is obtained.[19] The structure now becomes $LaAlO_3[MAl_{10}O_{16}]$, with the divalent cation substituting for an aluminum cation in the spinel block. This mechanism of charge balance leads to the ideal stoichiometric magnetoplumbite compounds $LnMAl_{11}O_{19}$, for Ln = La↔Gd, and M = Mg, Mn↔Zn, which have been used as laser and luminescent materials (see for example Ref. 19 and references therein).

The incongruent vaporization of alkali oxides decomposes alkali-stabilized β-aluminas above ~1000°C in open systems;[21,22] whereas incongruent vaporization is negligible in magnetoplumbites stabilized with alkaline-earth or rare-earth cations.[22,23] The magnetoplumbites are stable at temperatures well in excess of their proposed use in oxide CMCs. Therefore, the magnetoplumbites have received the most attention and are considered exclusively in this paper.

The mineral hibonite ($CaAl_{12}O_{19}$) occurs naturally in alluvial deposits and in metamorphosed limestones rich in calcic plagioclase, containing 3.2 wt% MgO, 8.5 wt% TiO_2, 2.3 wt% FeO, 0.45 wt% Fe_2O_3, and 1.5 wt% SiO_2.[24] Dayal and Glasser[25] showed that synthetic $CaAl_{12}O_{19}$ formed solid solutions with the hypothetical end member $CaFe_{12}O_{19}$, extending to ~70 mol% of the latter. Meteoritic hibonite typically contains substantial amounts of Mg, Ti, V, and Si.[26,27] The substitution mechanism is the replacement of Al^{3+} with an isovalent cation or the replacement of $2Al^{3+}$ with two charge-compensating aliovalent cations such that charge neutrality is maintained. For example, binary and ternary solid-solution hibonites have been produced in the $CaAl_{12}O_{19}$–$CaAl_{10}MgSiO_{19}$ and $CaAl_{12}O_{19}$–$CaAl_{10}MgSiO_{19}$-$CaAl_{10}MgTiO_{19}$ systems, respectively, with up to 15 mol% $CaAl_{10}MgSiO_{19}$ and 34 mol% $CaAl_{10}MgTiO_{19}$ (up to 1.7 wt% SiO_2, 3.6 wt% MgO, and 5.2 wt% TiO_2) with the most Si-rich hibonites restricted to the binary system.[28] The effect of impurities as controlled dopants on the synthesis and grain growth of calcium and lanthanum hexaluminates is discussed further in Sections 4 and 5.

Hexaluminates have basal plane cleavage that is qualitatively inferior to that of micas, graphite, and BN.[29] Preferred cleavage occurs at the weakly bonded inter-spinel layers (see Fig. 1). It is not known if there are significant differences in cleavage between the different hexaluminates. However, high fracture-energy anisotropy, with values which differ by a factor of 100, has been demonstrated in the β-aluminas[30,31] and there is evidence that magnetoplumbite fiber–matrix interlayers cleave sufficiently well to deflect matrix cracks in CMCs with single-crystal alumina and YAG fibers, but evidence for fiber pullout after crack deflection is still

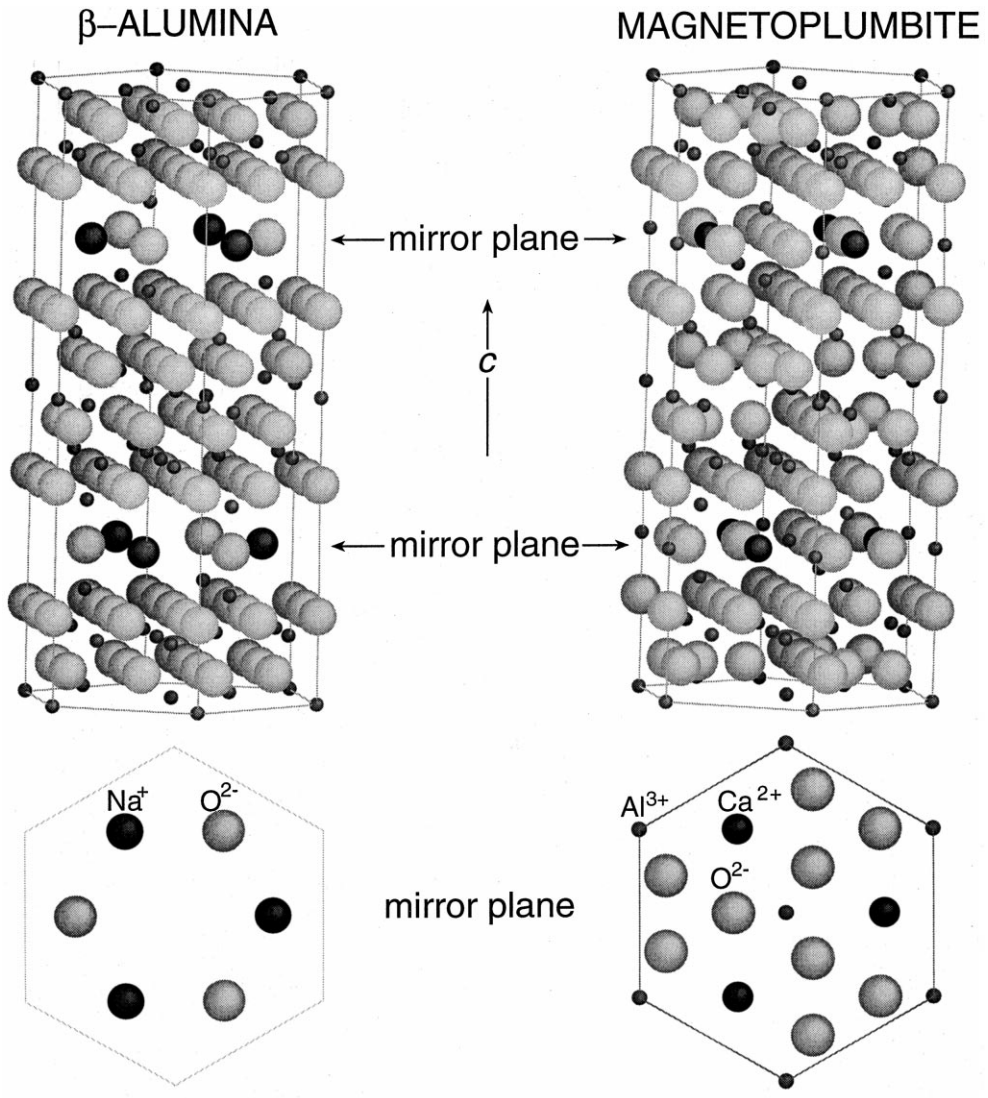

Fig. 1. β-Alumina and magnetoplumbite structures. Mirror planes viewed along the *c*-axes are given below each structure.

insubstantial.[32–36] Strain-energy release rates of 2.2 J/m^2 were measured of a highly textured polycrystalline $CaAl_{12}O_{19}$ layer between two alumina sheets.[33] SEM, EDS, and X-ray diffraction indicated that the crack propagated transgranularly by cleavage of the hibonite grains, rather than at the hibonite alumina interface. Specific examples are given in Section 5.3.

3. Issues in coating polycrystalline fiber tows

The application of coatings to fibers, more often than not, compromises their strength.[37,38] Often this is a result of the coating process and often this is due to the presence of the coating itself. Most oxide coatings are applied at temperatures greater than 1000°C to ensure complete reaction and conversion of the precursor to the desired phase and to fully sinter the coating onto the fiber. Most commercially available oxide fibers (Nextel 610 and 720, 3M) begin to lose strength at these temperatures due to grain growth. Also, during the coating process, compounds volitalize as byproducts and may act to weaken the fibers via a stress-corrosion mechanism. Fibers can also be weakened if they react with the precursor or the intermediate products during the coating process. If the coating has a significantly lower coefficient of thermal expansion than the fiber and remains strongly bonded, tensile stresses at the fiber–coating interface can lead to lower strengths. The presence of imperfections in the coating, such as excess material bridging individual filaments can also lead to problems. Liquid-phase precursors often form bridges of coating between filaments in a tow that later break during handling. The influence of bridges on composite processing and properties has yet to be fully explored. In the worst case, where bridges are extensively linked,

they can lead to failure of the tow during handling, impede infiltration of matrix, greatly increasing void space and severely reducing matrix strength. Linked bridges may also be a source of low-energy crack propagation through a bundle of fibers.

Issues specific to hexaluminate interphases include synthesis, microstructure and texture, and the process of coating fibers and texturing the interphase. To coat fine diameter polycrystalline alumina-based fibers with a textured hexaluminate coating, a precursor must have the following properties. First, the precursor must wet and completely infiltrate the fiber tow. The first requirement makes the use of nonaqueous precursors attractive with respect to obtaining sols with good wetting characteristics, although viscosities can be higher.[39] Second, the viscosity of the precursor should remain low at the desired concentrations for infiltration and deposition of coatings of adequate thickness and allow for ready displacement of the excess sol. Third, the precursor should yield the desired hexaluminate at temperatures below those at which the fibers begin to degrade. Commercially available polycrystalline alumina fibers (Nextel 610, 3M) are limited to processing temperatures of 1200°C to avoid significant grain growth that can lead to lower strengths. Precursor constituents can also diffuse into the fibers and accelerate degradation. In the case of hibonite, where CaO is present in the precursor, CaO can readily segregate to the grain boundaries of the fiber and lead to strength reduction, since CaO is known to embrittle alumina.[40–44] Finally, significant abnormal grain-growth of calcium hexaluminate must occur to obtain a coating with basal plane texture. The two most critical issues with respect to the application of hexaluminate coatings onto polycrystalline fibers need to be addressed to further research of these materials as potential fiber–matrix interphases and to validate the concept. The first is the lowering of the temperature of hexaluminate formation. The second is increasing grain growth to achieve basal texture at these lowered temperatures.

4. Synthesis from sol and solution presursors

4.1. Calcium hexaluminate

The reaction of CaO and Al_2O_3 generally proceeds dynamically in a nonequilibrium manner with the formation of calcia-rich aluminates, followed by the formation of the relatively calcia-poor aluminates, until eventually the stoichiometric calcium aluminate is formed.[45–47] For the case of CaO and Al_2O_3 in a 1:6 ratio, monocalcium aluminate and/or calcium dialuminate usually forms before the hexaluminate as follows[34,48–50]

$$CaO + Al_2O_3 \rightarrow CaAl_2O_4 \quad (1)$$

$$CaO + 2Al_2O_3 \rightarrow CaAl_4O_7 \quad (2a)$$

$$CaAl_2O_4 + Al_2O_3 \rightarrow CaAl_4O_7 \quad (2b)$$

$$CaAl_4O_7 + 4Al_2O_3 \rightarrow CaAl_{12}O_{19} \quad (3)$$

Residual $CaAl_4O_7$ and Al_2O_3 often accompany $CaAl_{12}O_{19}$ in the final product. In cases where $\leqslant 5$ wt% CaO was added to ~500-nm particle size α-Al_2O_3 powders, reactions (1) and (2) preceded reaction (3).[48,49] Whereas, in the case where the appropriate amount of a Ca-salt was added to 40-nm particle size (5-nm crystallites) boehmite to form a stoichiometric $CaO{:}6Al_2O_3$ colloidal sol, or the precursor was a polymeric solution, only reaction (2a) was found to precede reaction (3).[34,50] In general, the completion of such reactions depends on the diffusion distances, i.e. particle size and degree of mixing of the reactant powders.

The precursor sol originally used to apply coatings to single-crystal alumina and YAG fibers and plates was a boehmite colloid, doped with a stoichiometric amount of calcium acetate, which required temperatures of over 1400°C for complete reaction to hibonite and to fully texture the coating.[32–35] Coating polycrystalline alumina-based fibers with this same colloidal sol resulted in severe embrittlement of the fiber and the formation of an α-Al_2O_3 coating. Prior to the formation of calcium hexaluminate, CaO diffuses out of the coating and to the grain boundaries in the fiber, leaving an alumina-rich precursor behind. The viscous nature of the sol, which results from doping aqueous boehmite sols with even low levels of metal salts leads to extensive bridging of the filaments in the tow, despite the use of an immiscible liquid to remove excess sol during the coating process.

Many alternate precursors have been investigated including other colloidal based sols, organometallics, and polymeric solutions.[50] However, only one sol, a mixed-metal citric acid complex, was found to significantly lower the reaction temperature to yield hibonite, free of any intermediate phases, at 1300°C (Fig. 2). The resin that is formed during the condensation reaction with ethylene glycol is amorphous and contains the Ca^{2+} and Al^{3+} cations uniformly distributed on a very fine scale. The short diffusion distances between constituents and their uniform, stoichiometric dispersion gives rise to enhanced reactivity. The formation of the kinetically favored intermediate $CaAl_4O_7$, which must then react with Al_2O_3 to form $CaAl_{12}O_{19}$, seems to be suppressed during heating of the citrate-based precursor. However, even with a reaction temperature of 1300°C, significant degradation of polycrystalline fibers occurs.

It is well known that dopants in the form of solid-solution and liquid-phase formers can enhance the sintering

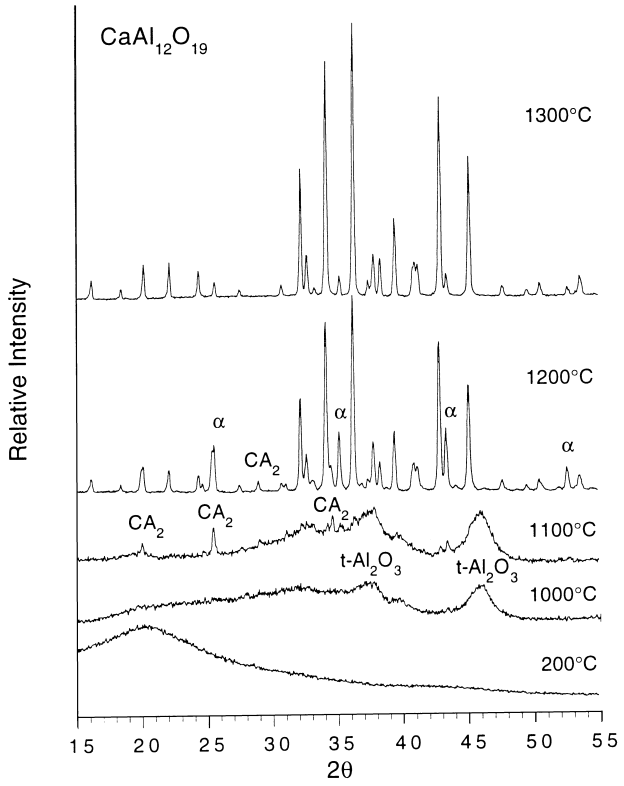

Fig. 2. XRD patterns of citrate-gel $CaAl_{12}O_{19}$ precursor after heating for 1 h in air at the indicated temperatures. Peaks not attributed to hibonite are labeled: t-Al_2O_3: a transitional alumina, CA_2: calcium dialuminate, α: corundum.

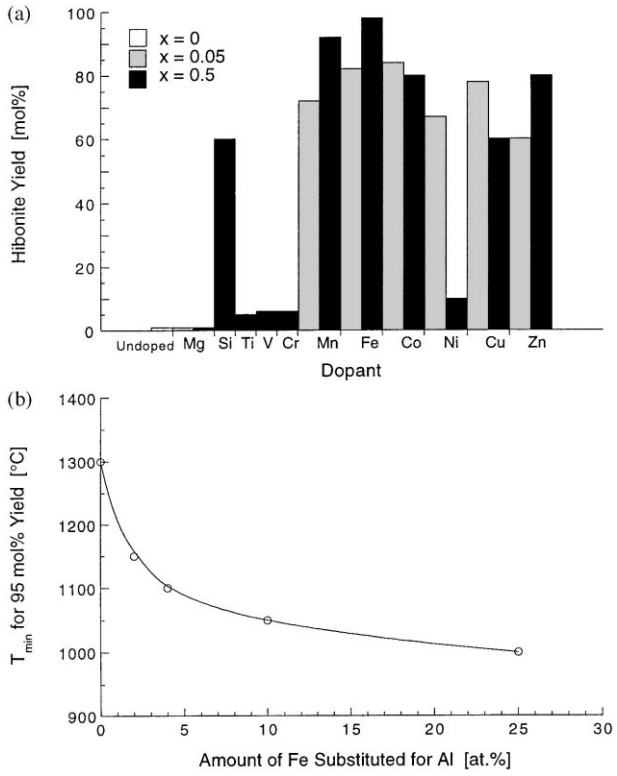

Fig. 3. (a) $CaM_xAl_{12-x}O_{19}$ yield for $x=0.5$ and 0.05 (4.0 at%- and 0.4 at%-doped citrate-based precursors) after 1 h at 1100°C. (b) Minimum temperature for obtaining phase-pure (>95 mol%) $Ca(Al,Fe)_{12}O_{19}$ within 1 h as a function of amount of Fe_{3+} substituted for Al_{3+}.

and grain growth,[51–60] creep,[61–64] and the γ→α phase transformation of alumina.[57,59] Dopants were incorporated into the citrate-based $CaAl_{12}O_{19}$ sol to investigate their effects on hibonite formation at 1100°C.[50] Incorporation of dopants into the citrate-based precursors significantly affected formation of calcium hexaluminate; in some cases it was suppressed, while in most of the others the extent of formation was increased dramatically under identical heat treatments [Fig. 3(a)]. Whether or not this was due to a solid-solution effect is not clear. While a second phase was detected by XRD only in the CoO-, NiO-, CuO-, or ZnO-doped powders, the other dopants could have either segregated to the grain boundaries or formed a lower-volume-fraction amorphous second phase, not readily detectable by XRD. Fe was added at levels of up to 25 at% to exploit the large solubility of Fe_2O_3 in $CaAl_{12}O_{19}$, resulting in a continuous decrease in formation temperature with increasing Fe substitution for Al [Fig. 3(b)].

With the doped-citrate powders, the γ→α phase transformation of alumina was enhanced in every case at 1100°C with the exception of the MgO-doped powder. For the powders doped at 4 at% with Ti, V, Mn, Fe, Co, and Cu the transformation to α-Al_2O_3 appeared to be complete. The suppression of α-Al_2O_3 formation, except in the case of MgO-doped powder, favors calcium aluminate formation. Ironically, most of the dopants that enhanced the formation of $CaAl_{12}O_{19}$ also are reported to lower the γ→α phase transformation temperature of alumina, with the exception of SiO_2.[59,65–68] The positive influence of the dopants on calcium hexaluminate formation is believed to be the enhanced reactivity of CaO with Al_2O_3 to form $CaAl_{12}O_{19}$ rather than $CaAl_4O_7$, prior to destabilization of the γ-Al_2O_3 spinel structure. The cations that resulted in the greatest hexaluminate yield at 1100°C are all known to stabilize the spinel structure, MAl_2O_4.

4.2. Lanthanum hexaluminate

Similar to the case of $CaAl_{12}O_{19}$, La_2O_3 reacts with Al_2O_3 to form an intermediate, in this case a perovskite, first:[39,69,70]

$$La_2O_3 + Al_2O_3 \rightarrow 2LaAlO_3 \quad (4)$$

$$LaAlO_3 + 5Al_2O_3 \rightarrow LaAl_{11}O_{18} \quad (5)$$

The formation of $LaAl_{11}O_{18}$ can be enhanced by the use of precursors with improved chemical homogeneity and decreased diffusion distances, compared with conventional mixing of elemental powders.[70] Ropp and

Carroll[69] have proposed that the rate limiting step in the reaction to $LaAl_{11}O_{18}$ is the conversion of O_2 to $2O^{2+}$, that accompanies La^{3+} diffusion.[71,72] Jero et al.[73] have found that the formation of $LaAl_{11}O_{18}$ from metallorganic precursors is enhanced in oxygen and hindered in argon, compared with air. Saruhan and co-workers[74,75] have recently reported the synthesis of $LaAl_{11}O_{18}$ at 1300°C in air by seeding a metallorganic sol with $LaAl_{11}O_{18}$ particles. While improved reactivity has been shown, phase-pure $LaAl_{11}O_{18}$ has not been obtained at temperatures below 1300°C.

As discussed earlier, substituting a divalent cation for one Al^{3+} in $LnAl_{11}O_{19}$ establishes charge balance and stabilizes the magnetoplumbite structure, producing lanthanide hexaluminate of the type $LnMAl_{11}O_{19}$, for Ln = La→Gd, and M = Mg, Mn→Zn. The easier preparation of the doped materials is attributed to the enhanced stabilization of the spinel blocks by the divalent cations, which reduce the number of vacancies in the unit cell, resulting in a stoichiometric magnetoplumbite. All of the divalent cations that stabilize the lanthanide-hexaluminate magnetoplumbites are also those whose oxides (MO) form spinel-type (MAl_2O_4) phases with alumina. $LaMnAl_{11}O_{19}$ and $LaCuAl_{11}O_{19}$ have been found to form completely at temperatures as low 1000°C from citrate-gel precursors, without the appearance of the intermediate perovskite, while La $MgAl_{11}O_{19}$, $LaFe_{1.5}Al_{10.5}O_{19}$, $LaCoAl_{11}O_{19}$, and La $ZnAl_{11}O_{19}$ form directly at 1100°C within 1 h without residual $LaAlO_3$ (Fig. 4).[39] Unlike its effect on calcium hexaluminate, where Fe_2O_3 was found to be most effective at enhancing crystallization of the magnetoplumbite, greater concentrations were necessary to produce phase-pure Fe-doped lanthanum hexaluminate at 1100°C. One reason for this is likely to be that the favored oxidation state of iron at these temperatures is 3+, rather than the required 2+.

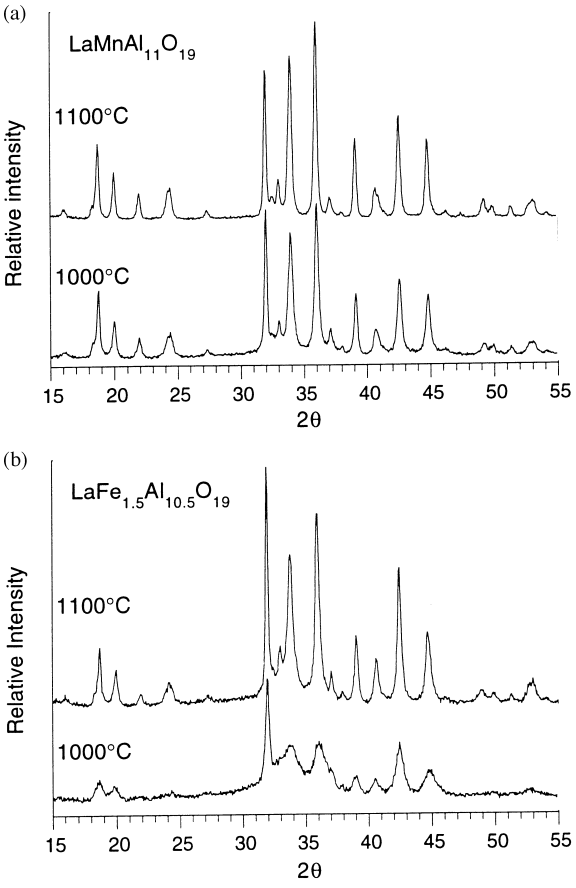

Fig. 4. XRD patterns of (a) $LaMnAl_{11}O_{19}$ and (b) $LaFe_{1.5}Al_{10.5}O_{19}$ powders heated at 1000 or 1100°C for 1 h.

5. Films and interphases

5.1. Development of texture in films and interphases

Near perfect texture of calcium and lanthanum hexaluminate films and interphases has been obtained on single-crystal substrates, as determined from XRD of films on plates (Fig. 5) and TEM of fiber coatings and interphases in composites (Fig. 6). Several mechanisms have been presented that could explain the 0001-textured $CaAl_{12}O_{19}$ free-standing films and coatings on single-crystal plates and fibers.[34] These include: (i) faster reaction along basal plane directions, geometric constraint of those grains not oriented for rapid growth, and subsequent seeding of abnormal grain growth by the initially larger size of the basal-oriented grains; (ii) rapid lattice diffusion along basal planes that partially constrain grain orientation when its formation is preceded by epitaxial seeding of alumina; and (iii) abnormal grain growth driven by surface/interface-energy anisotropy. In the case where the film was either free-standing or the substrate was not involved in the reactions, the low surface-energy (0001) planes of the hexaluminate were favored and abnormal grain-growth proceeded to form 0001-textured films without the aid of preferred reaction direction. Enhanced basal texture can be achieved by increasing abnormal grain growth by enhancing grain-boundary mobility, thinning the film, increasing surface/interface-energy anisotropy, and increasing the relative grain size of basal oriented grains to those in other orientations.

Grain growth can be significantly affected by the presence of impurities. Dopants may modify the lattice defect structure of the host, segregate to grain boundaries, or form a second phase (amorphous or crystalline) at the grain boundaries. The mobility of grain boundaries can be either reduced by solutes due to an interaction energy between grain boundaries and the solutes (solute drag),[76] or increased by an enhancement of diffusive mass-transport of the rate-limiting species.[77] Significant amounts of insoluble dopants can also give rise to grain boundaries that are either partially or completely

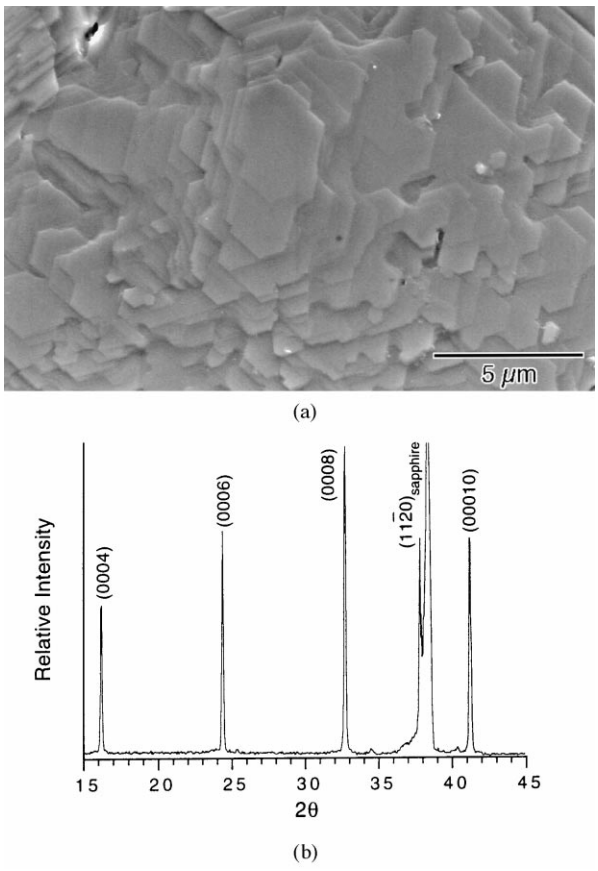

Fig. 5. (a) SEM image of textured $CaAl_{12}O_{19}$ on single-crystal alumina plate after heating to 1400°C for 2 h; (b) XRD pattern of hibonite coating.

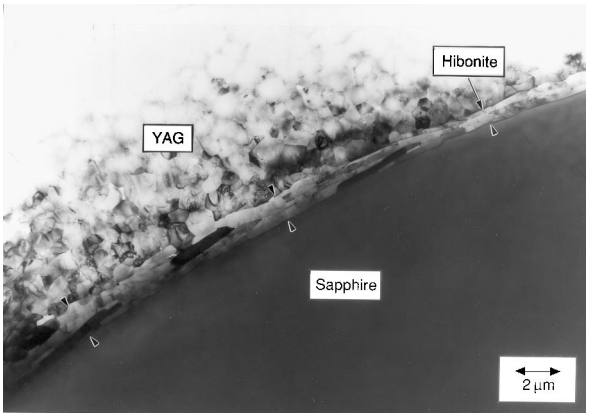

Fig. 6. TEM image of textured hibonite interphase between a single-crystal alumina fiber and polycrystalline YAG matrix, oriented along the fiber axis.

wetted, which can lead to increased abnormal grain growth.[56,58] Spin coated films of doped calcium and lanthanum hexaluminates on YAG have shown enhanced texture at temperatures below those obtainable with undoped films (Fig. 7).[39,50]

In the above examples highly textured films and interphases have been observed on single-crystal alumina

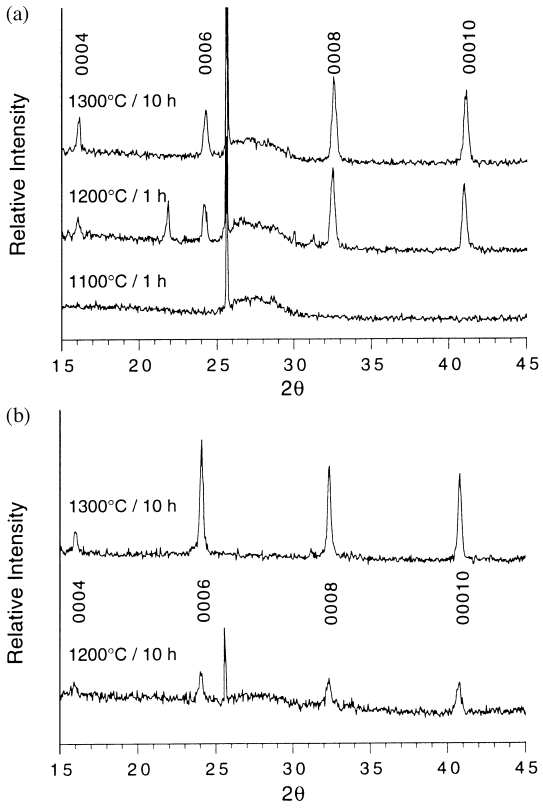

Fig. 7. XRD patterns of spin-coated (a) $CaFe_{0.5}Al_{11.5}O_{19}$ and (b) $LaFe_{1.5}Al_{10.5}O_{19}$ films onto (111) YAG. The films begin to texture at 1200°C, with only (0001) peaks present.

only at temperatures above 1400°C. Textured films have been obtained by annealing doped spin-coated films on single-crystal YAG at 1200°C.[39,50] In the latter case the use of an inert substrate, which does not interact with the film by seeding grain growth, results in enhanced reaction and texture. Similarly, self-supporting films can be highly textured at 1200°C when they are extremely thin.[39,50]

5.2. Coatings on polycrystalline fibers

In Section 3, issues germane to the application of a textured hexaluminate interphase were presented. Many of these issues do not pertain to the coating of single-crystal and monofilament fibers, such as the Saphikon single-crystal alumina fibers that were used in earlier work.[32–35] In this section some of these issues are addressed as a result of work on solution-derived calcium and lanthanum hexaluminates, and their application to alumina polycrystalline fibers.

To date basal-plane textured coatings have not been obtained on polycrystalline fibers. Early work on coating polycrystalline fibers with boehmite-based precursors to $CaAl_{12}O_{19}$ showed a severe degradation of fiber strength after coating. While even dilute sols were used to minimize fiber bridging, the apparent tow strength was still greatly reduced. Fig. 8 shows the

results of single-filament tensile tests from Nextel 610 tows after soaking in various dilute salt solutions and then heating at 1000°C for 10 h. While the strength of fibers soaked in the alkaline-earth nitrates were much lower than a control sample (heated but not exposed to solutions), the fibers exposed to lanthanum nitrate were not degraded. More recent work indicates that at 1100°C lanthanum nitrate-treated Nextel 610 also shows some degradation. This agrees with the effects of some of these cations on polycrystalline alumina reported in the literature.[40–44] These results suggest that lanthanum hexaluminate is preferred to calcium hexaluminate as a fiber coating to minimize strength loss of the fiber. Furthermore, La_2O_3 segregated to the grain boundaries of polycrystalline alumina has been reported to increase its creep resistance.[78]

The medium used for citric acid based polymeric solutions has a significant effect on viscosity. Fig. 9 shows the results of varying citric acid concentration on aqueous- and ethanol-based lanthanum hexaluminate precursor solutions. While not quantified, viscosities of ~2 cP seem to provide the best coatings with the least amount of bridging. However, precursors using ethanol seem to wet the fibers better than those using water as a solvent. The following coatings were applied with ethanol-based citric-acid polymeric solutions.

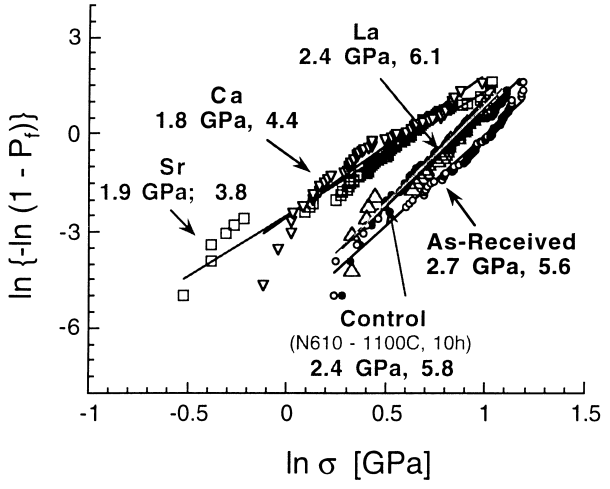

Fig. 8. Weibull plot of single-filament tensile tests of Nextel 610 fibers after heating tows exposed to various dilute nitrate solutions at 1000°C for 10 h (courtesy T.A. Parthasarathy).

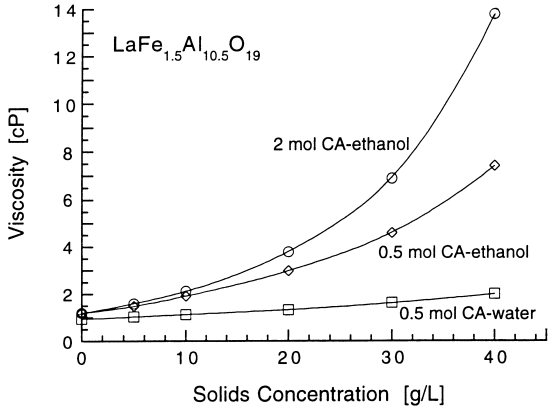

Fig. 9. Plot of viscosity as a function of solids concentration of $LaFe_{1.5}Al_{10.5}O_{19}$ solutions at 23°C. Solutions were synthesized with either 0.5 or 2 mol citric acid (CA) per mol of aluminum in water or ethanol as indicated.

Nextel 610 and 720 fibers have been coated with 30-g/l $CaFe_{0.5}Al_{11.5}O_{19}$ (CAF) and $LaFe_{1.5}Al_{10.5}O_{19}$ (LAF) solutions using a continuous fiber coater[79] and passed through an 1100°C furnace, positioned in series with the coater, at ~1 cm/s. Hexadecane, immiscible with ethanol, was floated on top of the sol to aid in removal of excess sol from between filaments, as discussed previously. Surfaces of coated fibers were characterized by SEM and epoxy-impregnated coated fibers were characterized by TEM.[80]

Nextel 610 and 720 fibers coated with CAF at 1100°C resulted in very uniform coatings on selected fibers, but were often not present on all filaments; coatings ranged from 0 to 200 nm in thickness. Selected-area electron diffraction of coatings on fibers gave diffuse rings that were indexed as nanocrystalline θ-Al_2O_3 [Fig. 10(a)]. EDS of the coatings indicated the presence of Ca in some of the coatings, but not all, whereas, Fe was present in all coatings. Heat treating the coated fibers for 1 h at 1100°C resulted in a well crystallized α-$(Al,Fe)_2O_3$ coating [Fig. 10(b)]. No Ca could be detected within the coating. After heating at 1200°C for 10 h, large elongated grains of $(Al,Fe)_2O_3$ (due to CaO in amounts below the EDS detection limit) could be seen oriented with the basal planes growing radially outward from the fiber, as though seeded by the fiber surface or simply due to a radial reaction direction or grain growth within the coating.

Nextel 610 fiber tows were also coated with LAF at 1100°C. TEM of the as-coated fibers indicated that the coating was a nanocrystalline magnetoplumbite. EDS confirmed the presence of La and Fe. After heating at 1100°C for 1 h the grains in the coating had significantly coarsened but the composition had remained the same. After heating at 1200°C for 10 h, some texturing was evident with grains in a similar orientation as those observed in the CAF-coated fibers. Fig. 11 shows the coatings on the fibers as coated and after heating for 10 h at 1200°C.

While basal-textured coatings were not obtained with either compound on Nextel 610 fibers, the lanthanum hexaluminate phase was formed. Texture development is believed to require temperatures in excess of those used in this work due to the interaction of the fiber with reaction and grain growth in the coating, which can initiate growth directions outward from the fiber surface as shown in Figs. 10(b) and 11(b). Unfortunately, at greater temperatures, the reduction in fiber strength is

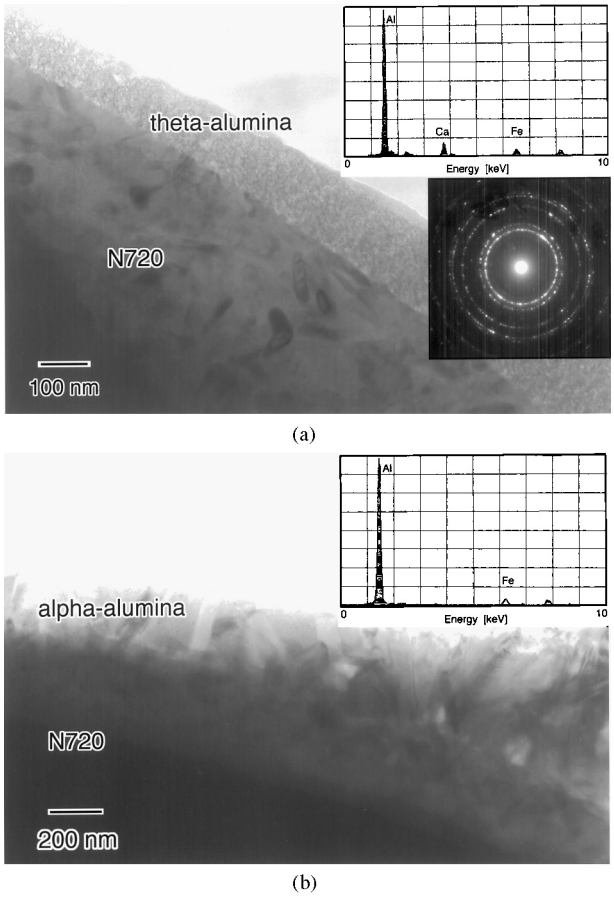

Fig. 10. TEM images of Nextel 720 fibers containing coatings applied with the iron-doped calcium hexaluminate citrate precursor: (a) fiber coated at 1100°C (15 s residence time). EDS spectrum of the coating indicates presence of Ca and Fe (peak at 8.05 keV is Cu from ion milling). SAD pattern identifies the coating as being composed of q-$(Al,Fe)_2O_3$; (b) fiber coating after heating for 1 h at 1100°C, with grains of α-$(Al,Fe)_2O_3$ growing radially outward from the fiber surface with basal planes normal to the plane of the interface. Similar results were obtained with Nextel 610 fibers.

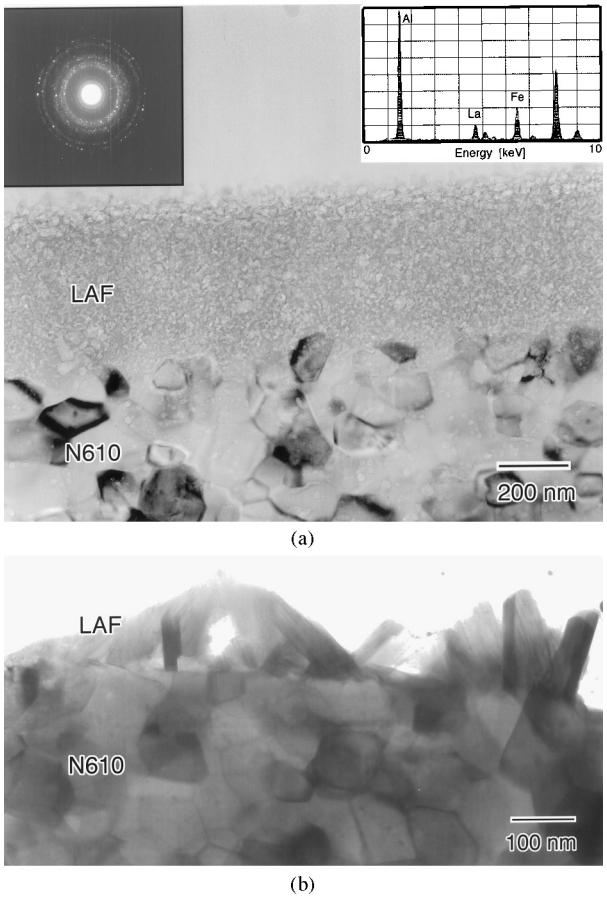

Fig. 11. TEM images of Nextel 610 fibers containing coatings applied with the iron-doped lanthanum hexaluminate citrate precursor: (a) fiber coated at 1100°C (15 s residence time). EDS spectrum of the coating indicates presence of La and Fe. SAD pattern identifies the coating as $LaFe_{1.5}Al_{10.5}O^{19}$; (b) fiber coating after heating for 10 h at 1200°C, with magnetoplumbite grains growing radially outward from fiber surface, with basal planes approximately normal to the plane of the interface. Large peak at 8.05 keV in spectrum is Cu sputtered during ion milling.

much greater still and would not result in a useful fiber, let alone a useful coated fiber.

5.3. Crack-interphase interaction in model composites

To date, coatings on model composites using single-crystals as one or more of the constituents are the only evidence that has been presented in support of hexaluminates as a viable cleavable oxide fiber coating. The earliest encouraging results came from the observation of cracks that had been deflected within a $CaAl_{12}O_{19}$ interphase and propagated around a fiber via transgranular cleavage in a TEM foil.[32–35] Subsequent work imaging the fracture surfaces of various model composites containing single-crystal alumina with textured $CaAl_{12}O_{19}$ coating clearly indicated crack deflection within the coating. However, it also indicated the relatively rough debond surface that results and is believed to give rise to extremely high radial compressive stresses upon sliding, which results in minimal fiber pull-out.[81,82,83] Fig. 12 illustrates these features rather well. The coating can be seen bonding to both the fiber and matrix in the region surrounding the partially debonded fiber. Flat cleavage fracture can be seen, yet due to the presence of grain boundaries where the crack can also propagate intergranularly the surface is rather rough. This is also believed to be the reason why fibers coated with textured hibonite cannot be pushed out of a matrix.[33] Simple geometric arguments suggest that the minimum roughness amplitude, A, for intragranular cleavage fracture must depend on the hexaluminate grain size, d, and the fiber diameter, r_f,[83]

$$A = (r_f^2 + d^2)^{1/2} - r_f$$

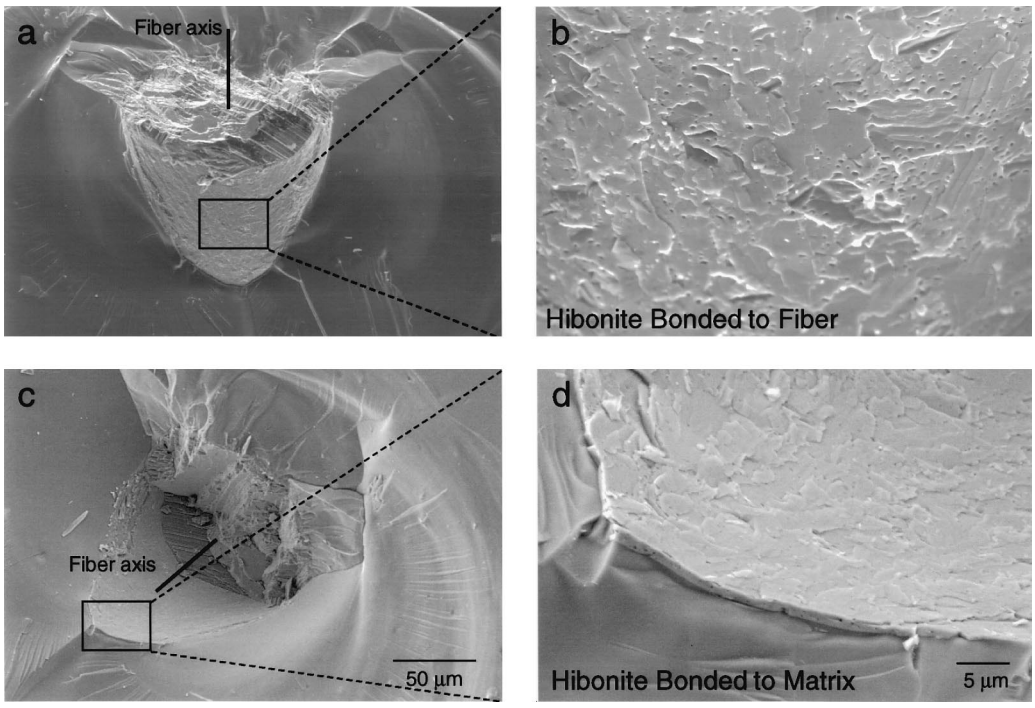

Fig. 12. SEM images of two mating fracture surfaces from a tape-cast composite consisting of textured-hibonite-coated sapphire fibers in a potassium–borosilicate glass matrix. (a) and (c) show two halves of the fiber, which is partially debonded from the matrix. Higher magnification images in (b) and (d) show interphase bonding to fiber and matrix, respectively, indicating crack deflection and propagation within the fiber coating. Note flat cleavage features and rough surface due to intergranular stepping of crack at grain boundaries.

Low roughness amplitudes that allow fiber pullout after debonding require $d << r_f$, but may also require thin interlayers that force d to be small, and limit large intergranular jumps in the fracture path between grains that may cause much larger roughness amplitudes. Coating thicknesses less than 0.2 mm and grain sizes larger than 10 μm are suggested for significant debond lengths on 140-μm diameter fibers. This dictates a monolayer of plate-shaped grains with an aspect ratio of <0.02, which is approximately an order of magnitude less than that currently observed in hibonite coatings on sapphire (see Fig. 6).

Tensile tests of microcomposites, which contain a single 135-μm diameter sapphire fiber coated with a textured hibonite interlayer and an outer layer of polycrystalline alumina as the matrix indicated that there was no perceptible nonlinearity in the load–diplacement plot (Fig. 13).[36] However, the compliance of the microcomposites was lower than that of bare sapphire fibers, indicating significant load transfer occurred. While the median strength of the hibonite-containing microcomposites was the same as that of microcomposites without an hibonite interphase, the Weibull modulus was nearly three times greater, which suggests that the hibonite was protecting the fibers from matrix cracks. SEM of the fracture surfaces revealed crack deflection within the hibonite fiber coating; however, debond lengths were limited to a few micrometers.

6. Compatability with potential CMC phases

Hexaluminates are the most alumina-rich aluminates that form and, therefore, are phase compatible with alumina. Incongruent melting points for the magnetoplumbite-structured hexaluminates have been reported to range from 1833[84] to 1883°C[85] for $CaAl_{12}O_{19}$ and from 1848[86] to 1930°C[87] for $LaAl_{11}O_{18}$. Calcium hexaluminate has been shown to be stable with YAG up to at least 1650°C;[32–35] lanthanum hexaluminate is also phase compatible with YAG.[39] While the various doped calcium and lanthanum hexaluminates have not been

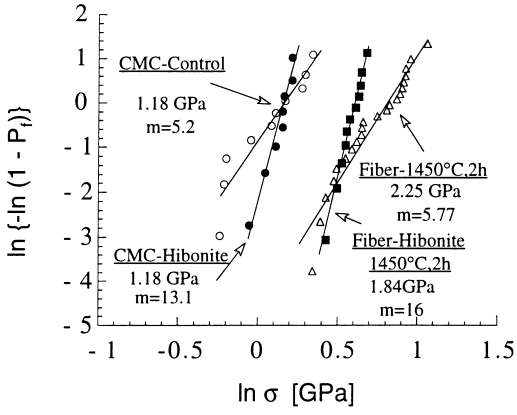

Fig. 13. Weibull plot comparing tensile test results of microcomposites and fibers with and without a hibonite fiber coating.

found to react with either alumina or YAG, there is likely to be some segregation of these dopants to form solid solutions and/or concentrate at grain boundaries, especially in the case of Fe, which is highly soluble in Al_2O_3 and YAG. The degree to which this is a potential problem with respect to altering the strength and creep resistance of fibers is not known.

Cerium hexaluminate has been reported to be stable with both alumina and zirconia up to at least 1500°C in oxidizing atmospheres.[88,89] However, Longo and Podda[90] reported that $CeAl_{11}O_{18}$ was only stable above 1600°C in air and only at lower temperatures at lower oxygen partial pressures, where Ce^{4+} is reduced to Ce^{3+}. The only other reported phase diagrams containing phase relations between a hexaluminate and zirconia are those of the systems $BaO–Al_2O_3–ZrO_2$ and $CaO–Al_2O_3–ZrO_2$ which both indicate phase compatibility of the respective hexaluminate and ZrO_2.[91,92]

The hexaluminates are not stable with SiO_2 or mullite, according to the phase diagrams.[84,93] Fig. 14 contains the XRD results indicating the amount of hexaluminate remaining in an initial 14 mol% $LaAl_{11}O_{18}$–86 mol% mullite powder mixture after heating at temperatures of 1200–1400°C.[93] The reactions between hexaluminates and SiO_2 and mullite are likely to be kinetically limited at temperatures of <1000°C;[93,94] however, as discussed in the previous sections much higher temperatures are required to synthesize and texture these coatings.

Of the current commercially produced fibers, only Nextel 610 appears to be phase compatible with a hexaluminate fiber coating. It seems unlikely that hexaluminates could be used in high-temperature composites containing either mullite or SiC in air, primarily due to the potential for these phases to react at elevated temperatures. This eliminates all other commercially produced fibers, whether SiC-based (e.g. Nicalon and Tyranno) or containing mullite (Nextel 720). A potentially suitable fiber for these coatings is one composed of YAG. Not only is YAG a more refractory oxide than alumina,[95–97] it allows for texturing at lower temperatures, based on the work of coating single crystal YAG and alumina substrates with both calcium and lanthanum hexaluminates.[39,50]

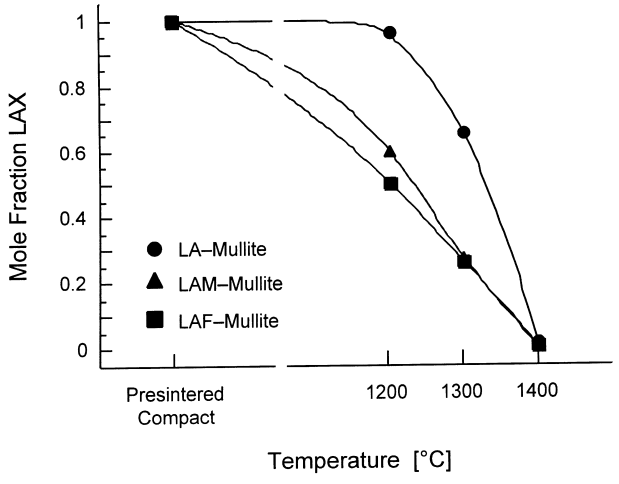

Fig. 14. Fraction of initial amount (14 mol%) of lanthanum hexaluminates present in lanthanum hexaluminate–mullite pellets after 24 h as a function of temperature. LA: $LaAl_{11}O_{18}$, LAM: $LaMnAl_{11}O_{19}$, and LAF: $LaFe_{1.5}Al_{10.5}O_{19}$.

7. Summary of current status and issues

Hexaluminates have been investigated as a cleavable oxide analogue to carbon and boron nitride fiber–matrix interphases. Highly textured coating and interphases have been produced on a variety of single-crystal fibers and plates at temperatures above 1400°C. The mechanism of microstructure development leading to a highly textured film has been presented. Examples of crack-interphase interaction and modes of debonding and crack propagation have been given. The current status with regard to the development of precursors for lower temperature synthesis and texturing of coatings on polycrystalline fibers and issues which need to be addressed are summarized below.

1. Phase-pure $CaAl_{12}O_{19}$ can be synthesized at 1300°C within 1 h. With dopants such as Fe_2O_3, $Ca(Al,Fe)_{12}O_{19}$ can be synthesized at 1000–1100°C.
2. $LaAl_{11}O_{18}$ can be synthesized at 1300°C when pure O_2 and metallorganic precursors are used. With dopants such as MnO, $LaMnAl_{11}O_{19}$ can be synthesized at 1000°C.
3. The rate of grain growth of $Ca(Al,Fe)_{12}O_{19}$ is about an order of magnitude faster than that of $La(Al,Fe)_{12}O_{19}$ at 1200°C. The rate of grain growth of doped powders is about and order of magnitude greater than that of undoped powders. The particular dopant does not greatly affect grain growth unless a transient liquid phase is formed.
4. The degree of texture may be influenced by dopants, at least on {111} YAG. Alumina substrates interact with the reaction of coating precursor and/or subsequent grain-growth, increasing the minimum temperature for texturing.
5. Hexaluminates are thermodynamically compatible with alumina, YAG, and ZrO_2, but not mullite. Dopants in hexaluminates greatly enhance the reaction with mullite. The reaction between $LaAl_{11}O_{18}$ and mullite is probably kinetically limited at temperatures below ~1000°C.
6. Strengths of polycrystalline alumina fibers exposed to calcium and strontium nitrates and then heated to 1000°C are degraded, but those of fibers exposed to lanthanum nitrate are not. At 1100°C

all cations degrade fiber strength to some extent. The effects of other dopants on various properties (strength, creep, etc.) of fiber and matrix phases has not been explored.

7. During application of either a $CaAl_{12}O_{19}$ or $Ca(Al,Fe)_{12}O_{19}$ precursor to polycrystalline fibers, CaO segregation to the fiber occurs, resulting in the formation of an Al_2O_3 coating.
8. During application of a $LaFe_{1.5}Al_{10.5}O_{19}$ precursor to polycrystalline fibers, La_2O_3 segregation is minimal and a $LaFe_{1.5}Al_{10.5}O_{19}$ coating is obtained.
9. Texture has not been obtained on any polycrystalline fiber. With the current alumina-based fibers synthesis and texture of the hexaluminate coating must occur at $\leqslant 1200°C$. Preferred orientation during nucleation is likely to be required to obtain a highly textured coating on these fibers due to temperature constraints.

Acknowledgements

I thank R.S. Hay, T.A. Parthasarathy, R.J. Kerans, R.E. Dutton, T. Mah, and P.D. Jero for assistance and/or helpful discussions on various aspects of this work.

References

1. Grathwohl, G., Kunz, M., Pippel, E. and Woltersdorf, J., The real structure of the interlayer between fibre and matrix and its influence on the properties of ceramic composites. *Physica. Status Solidi*, 1994, **A146**, 141–393.
2. Brennan, J. J., Interfacial chemistry and bonding in fibre reinforced glass and glass–ceramic matrix composites. In *Ceramic Microstructures '86: Role of Interfaces*, ed. J. A. Pask and A. G. Evans. Plenum Press, New York, 1987, pp. 387–399.
3. Brennan, J. J., Interfacial studies of chemical-vapor infiltrated ceramic matrix composites. *Mater. Sci. Eng.*, 1990, **A126**, 203–223.
4. Cooper, R. F. and Chyung, K., Structure and chemistry of fibre–matrix interfaces in silicon carbide fibre-reinforced glass-ceramic composites: an electron microscopy study. *J. Mater. Sci.*, 1987, **22**, 3148–3160.
5. Ponthieu, C., Lancin, M. and Thibault-Desseaux, J., Comparative study of the microstructure of the interphase in two SiC fibre/lithium aluminosilicate matrix composites. *Phil. Mag. A.*, 1990, **62**, 605–615.
6. Chaim, R. and Heuer, A. H., The interface between (Nicalon) SiC fibres and a glass-ceramic matrix. *Adv. Ceram. Mater.*, 1987, **2**, 154–158.
7. Chaim, R., Brandon, D. G. and Baum, L., Mechanical properties and microstructural characterization of SiC-fibre-reinforced cordieritic glass-ceramics. *Ceram. Eng. Sci. Proc.*, 1988, **9**, 695–704.
8. Bischoff, E., Rühle, M., Sbaizero, O. and Evans, A. G., Microstructural studies of the interfacial zone of a SiC-fibre-reinforced lithium aluminium silicate glass-ceramic. *J. Am. Ceram. Soc.*, 1989, **72**, 741–745.
9. Cao, H. C., Bischoff, E., Sbaizero, O., Rühle, M., Evans, A. G., Marshall, D. B. and Brennan, J. J., Effect of interfaces on the properties of fibre-reinforced ceramics. *J. Am. Ceram. Soc.*, 1990, **73**, 1691–1699.
10. Brennan, J. J., Nutt, S. R. and Sun, E. Y., Interfacial microstructure and stability of BN coated Nicalon fibre/glass matrix composites. *Ceram. Trans.*, 1995, **58**, 53–64.
11. Naslain, R., Dugne, O., Guette, A., Sevely, J., Brosse, C. R., Rocher, J. P. and Cotteret, J., Boron nitride interphase in ceramic matrix composites. *J. Am. Ceram. Soc.*, 1991, **74**, 2482–2488.
12. He, M. Y. and Hutchinson, J. W., Crack deflection at the interface between dissimilar materials. *Int. J. Solids Struct.*, 1989, **25**, 1053–1067.
13. Cooper, R. F. and Hall, P. C., Reactions between synthetic mica and simple compounds with application to oxifidation resistant ceramic composites. *J. Am. Ceram. Soc.*, 1993, **76**, 265–273.
14. King, T. A. and Cooper, R. F., Ambient-temperature mechanical response of a fluoromica–alumina laminate. *J. Am. Ceram. Soc.*, 1994, **77**, 1699–1705.
15. Segadaes, A. M., Warren, P. D. and Evans, A. G., Preliminary assessment of mica as a high temperature fiber coating for SiC composites. In *Annual Report of University Research Initiative*. ONR/DARPA Contract No. N00014-92-J-1808, University of California, Santa Barbara, CA, 1993.
16. Deer, W. A., Howie, R. A. and Zussman, J., *An Introduction to the Rock Forming Minerals*. Longman Group, London, 1978, pp. 225–230.
17. Fair, G., Shemkunas, M., Petuskey, W. T. and Sambasivan, S., Layered perovskites as 'soft ceramics'. *J. Eur. Ceram. Soc.*, 1999, **19**, 2437–2447.
18. Iyi, N., Takekawa, S. and Kimura, S., The crystal chemistry of hexaluminates: β-alumina and magnetoplumbite structures. *J. Solid State Chem.*, 1989, **83**, 8–19.
19. Collongues, R., Gourier, D., Kahn-Harari, A., Lejus, A. M., Théry, J. and Vivien, D., Magnetoplumbite-related oxides. *Ann. Rev. Mater. Sci.*, 1990, **20**, 51–82.
20. Iyi, N., Inoue, Z., Takekawa, S. and Kimura, S., The crystal structure of lanthanum hexaaluminate. *J. Solid State Chem.*, 1984, **54**, 70–77.
21. Duncan, J. H. and Creyke, W. E. C., The formation and stability of β-alumina in α-alumina ceramics. *Trans. Br. Ceram. Soc.*, 1969, **68**, 137–144.
22. Cinibulk, M. K., Thermal stability of some hexaluminates at 1400°C. *J. Mater. Sci. Lett.*, 1995, **14**, 651–654.
23. Morgan, P. E. D. and Curin, E. H., The magnetoplumbite crystal structure as a radwaste host. *J. Am. Ceram. Soc.*, 1982, **65**, C-114–C-115.
24. Curien, H., Guillemin, C., Orcel, J. and Sternberg, M., Hibonite. *Am. Mineral.*, 1957, **42**, 119.
25. Dayal, R. R. and Glasser, F. P., In *Science of Ceramics*, Vol. 3, ed. G.H. Stewart. Academic Press,. New York, 1967, pp. 191–214.
26. Armstrong, J. T., Meeker, G. P., Huneke, J. C. and Wasserburg, G., The blue angel: I. The mineralogy and petrogenesis of a hibonite inclusion from the murchison meteorite. *Geochim. Cosmochim. Acta.*, 1982, **46**, 575–595.
27. Ireland, T. R., Fahey, A. J. and Zinner, E. K., Trace element abundances in hibonites from the murchison carbonaceous chrondrite: constraints on high-temperature processes in the solar nebula. *Geochim. Cosmochim. Acta*, 1988, **52**, 2841–2854.
28. Beckett, J. R. and Stolper, E., The stability of hobnite, melilite, and other aluminous phases in silicate melts: implications for the origin of hobnite-bearing inclusions from carbonaceous chondrites. *Meteoritics*, 1994, **29**, 41–65.
29. Phillips, W. R. and Griffen, D. T., *Optical Mineralogy — The Non-Opaque Minerals*. W.H. Freeman & Co., San Fransisco, 1981.
30. Hitchcock, D. C. and De Jonghe, L. C., Fracture toughness anistropy of sodium-β-alumina. *J. Am. Ceram. Soc.*, 1983, **66**, C204.
31. Morgan, P. E. D. and Marshall, D. B., Functional interfaces for oxide/oxide composites. *Mater. Sci. Eng.*, 1993, **A162**, 15–25.

32. Cinibulk, M. K., Magnetoplumbite compounds ass a fiber coating in oxide/oxide composites. *Ceram. Eng. Sci. Proc.*, 1994, **15**, 721–729.
33. Cinibulk, M. K., Microstructure and mechanical behaviour of an hibonite interphase in alumina-based composites. *Ceram. Eng. Sci. Proc.*, 1995, **16**, 633–641.
34. Cinibulk, M. K. and Hay, R. S., Textured magnetoplumbite fiber-matrix interphase derived from sol–gel fiber coatings. *J. Am. Ceram. Soc.*, 1996, **79**, 1233–1246.
35. Cinibulk, M. K., Hay, R. S. and Dutton, R. E., Textured calcium hexaluminate fiber–matrix interphase for ceramic-matrix composites. In *Ceramic Microstructures: Control at the Atomic Level*, ed. A. P. Tomsia and A. M. Glaeser. Plenum Press, New York, 1998, pp. 731–739.
36. Parthasarathy, T. A., Boakye, E., Cinibulk, M. K. and Petry, M. D., Fabrication and testing of oxide/oxide microcomposites with monazite and hibonite as interlayers. *J. Am. Ceram. Soc.*, 1999, **82**, 3575–3583.
37. Hay, R. S., Petry, D. and Boakye, E., Fiber strength with coatings from sols and solutions. *Ceram. Eng. Sci. Proc.*, 1996, **17**, 43–52.
38. Hay, R. S., Boakaye, E. and Petry, M. D., Effects of coating deposition temperature on monazite coated fiber. *J. Eur. Ceram. Soc.*, 2000, **20**(5), 589–597.
39. Cinibulk, M. K., Effect of divalent cations on synthesis of citrate-gel-derived lantanum hexaluminate powders and films. *J. Mater. Res.*, in press.
40. Funkenbusch, A. W. and Smith, D. W., Influences of Ca on the fracture strength of polycrystalline alumina. *Metall. Trans. A.*, 1975, **6A**, 2299–2301.
41. Jupp, R. S., Stein, D. F. and Smith, D. W., Observations on the effect of calcium segregation on the fracture behaviour of polycrystalline alumina. *J. Mater. Sci.*, 1980, **15**, 96–102.
42. de With, G. and Hattu, N., The influence of CaO-doping on the fracture toughness of hot-pressed Al_2O_3. *J. Mater. Sci.*, 1981, **16**, 841–844.
43. de With, G., Fracture of translucent alumina: temperature dependence and influence of CaO dope. *J. Mater. Sci.*, 1984, **19**, 2195–2202.
44. Cook, R. F. and Schrott, A. G., Calcium segregation to grain boundaries in alumina. *J. Am. Ceram. Soc.*, 1988, **71**, 50–58.
45. Kopanda, J. E. and MacZura, G., Production processes, properties, and applications for calcium aluminate cements. In *Alumina Chemicals Science and Technology Handbook*, ed. L. D. Hart. American Ceramic Society, Westerville, OH, 1990, pp. 171–184.
46. Singh, V. K., Ali, M. M. and Mandal, U. K., Formation kinetics of calcium aluminates. *J. Am. Ceram. Soc.*, 1990, **73**, 872–876.
47. Gülgün, M. A., Popoola, O. O. and Kriven, W. M., Chemical synthesis and characterization of calcium aluminate powders. *J. Am. Ceram. Soc.*, 1994, **77**, 531–539.
48. Wu, S. J., De Jonghe, L. C. and Rahaman, M. N., Subeutectic densification and second-phase formation in Al_2O_3–CaO. *J. Am. Ceram. Soc.*, 1985, **68**, 385–388.
49. An, L., Chan, H. M. and Soni, K. K., Control of calcium hexaluminate grain morphology in in-situ toughened ceramic composites. *J. Mater. Sci.*, 1996, **31**, 3223–3229.
50. Cinibulk, M. K., Effect of precursors and dopants on the synthesis and grain growth of calcium hexaluminate. *J. Am. Ceram. Soc.*, 1998, **81**, 3157–3168.
51. Smothers, W. J. and Reynolds, H. J., Sintering and grain growth of alumina. *J. Am. Ceram. Soc.*, 1954, **37**, 588–595.
52. Cahoon, H. P. and Christensen, C. J., Sintering and grain growth of alpha-alumina. *J. Am. Ceram. Soc.*, 1956, **39**, 337–344.
53. Keski, J. R. and Cutler, I. B., Effect of manganese oxide on sintering of alumina. *J. Am. Ceram. Soc.*, 1965, **48**, 653–654.
54. Bagley, R. D., Cutler, I. B. and Johnson, D. L., Effect of TiO_2 on initial sintering of Al_2O_3. *J. Am. Ceram. Soc.*, 1970, **53**, 136–141.
55. Rao, W. R. and Cutler, I. B., Effect of iron oxide on the sintering kinetics of Al_2O_3. *J. Am. Ceram. Soc.*, 1973, **56**, 588–593.
56. Kaysser, W. A., Sprissler, M., Handwerker, C. A. and Blendell, J. E., Effect of a liquid phase on the morphology of grain growth in alumina. *J. Am. Ceram. Soc.*, 1987, **70**, 339–343.
57. Shelleman, R. A. and Messing, G. A., Liquid-phase-assisted transformation of seeded γ-alumina. *J. Am. Ceram. Soc.*, 1988, **71**, 317–322.
58. Song, H. and Coble, R. L., Origin and growth kinetics of plate-like abnormal grains in liquid-phase-sintered alumina. *J. Am. Ceram. Soc.*, 1990, **73**, 2077–2085.
59. McArdle, J. L. and Messing, G. L., Transformation, microstructure development and densification in α-Fe_2O_3-seeded boehmite-derived alumina. *J. Am. Ceram. Soc.*, 1993, **76**, 214–222.
60. Tartaj, J. and Messing, G. L., Effect of the addition of α-Fe_2O_3 on the microstructural development of boehmite-derived alumia. *J. Mater. Sci. Lett*, 1997, **16**, 168–170.
61. Hollenberg, G. W. and Gordon, R. S., Effect of oxygen partial pressure on the creep of polycrystalline Al_2O_3 doped with Cr, Fe, or Ti. *J. Am. Ceram. Soc.*, 1973, **56**, 140–147.
62. Lessing, P. A. and Gordon, R. S., Creep of polycrystalline alumina, pure and doped with transition metal impurities. *J. Mater. Sci.*, 1977, **12**, 2291–2302.
63. Gordon, R. S., Understanding defect structure and mass transport in polycrystalline Al_2O_3 via the study of diffusional creep. In *Structure and Properties of MgO and Al_2O_3 Ceramics*, ed. W. D. Kingery. American Ceramic Society, Columbus, OH, 1984, pp. 718–737.
64. Cannon, W. R., High creep ductility in alumina containing compensating additives. In *Structure and Properties and MgO and Al_2O_3 Ceramics*, ed. W. D. Kingery. American Ceramic Society, Columbus, OH, 1984, pp. 741–749.
65. Iler, R. K., Effect of silica on transformations of fibrillar colloidal boehmite and gamma alumina. *J. Am. Ceram. Soc.*, 1964, **47**, 339–341.
66. Bye, G. C. and Simpkin, G. T., Influence of Cr and Fe on formation of α-Al_2O_3 from γ-Al_2O_3. *J. Am. Ceram. Soc.*, 1974, **57**, 367–371.
67. Xue, L. A. and Chen, I.-W., Influence of additives on the γ-to-α transformation of alumina. *J. Mater. Sci. Lett.*, 1992, **11**, 443–445.
68. Polli, A. D., Lange, F. F., Levi, C. G. and Mayer, J., Crystallization behaviour and microstructure evolution of $(Al,Fe)_2O_3$ synthesized from liquid precursors. *J. Am. Ceram. Soc.*, 1996, **79**, 1745–1755.
69. Ropp, R. C. and Carroll, B., Solid-state kinetics of $LaAl_{11}O_{18}$. *J. Am. Ceram. Soc.*, 1980, **63**, 416–419.
70. Cinibulk, M. K., Synthesis and characterization of sol–gel derived lanthanum hexaluminate powders and films. *J. Mater. Res.*, 1995, **10**, 71–76.
71. Kohatsu, I. and Brindley, G. W., Solid state reactions between CaO and α-Al_2O_3. *Z. Physik. Chemie N. F.*, 1968, **60**, 79–89.
72. Miura, M., Hongoh, H., Yogo, T., Hirano, S. and Fuji, T., Formation of plate-like lanthanum-β-alumina crystal in Ce-TZP matrix. *J. Mater. Sci.*, 1994, **29**, 262–268.
73. Jero, P. D., Rebillat, F., Kent, D. J. and Jones, J. G., Crystallization of lanthanum hexaluminate from MOCVD precursors. *Ceram. Eng. Sci. Proc.* 1998, **19**, 359–360.
74. Saruhan, B., Schneider, H., Komarneni, S. and Abothu, I. R., Electrostatically deposited surface seeding and promotion of crystallization of sol–gel derived $LaAl_{11}O_{18}$ coating on oxide fibers. *J. Eur. Ceram. Soc.*, 1999, **19**, 2427–2435.
75. Komarneni, S., Abothu, I. R., Saruhan, B. and Schneider, H., Fabrication of interphases on mullite fibers by sol–gel and nanocomposite processing. *J. Eur. Ceram. Soc.*, in press.
76. Cahn, J. W., The impurity-drag effect in grain boundary motion. *Acta. Metall.*, 1962, **10**, 789–798.

77. Readey, D. W., Transport and sintering in impure ionic solids. *J. Am. Ceram. Soc.*, 1966, **49**, 366–369.
78. Cho, J., Harmer, M. P., Chan, H. M., Rickman, J. M. and Thompson, A. M., Effect of yttrium and lanthanum on the tensile creep behaviour of aluminum oxide. *J. Am. Ceram. Soc.*, 1997, **80**, 1013–1017.
79. Hay, R. S., Sol–gel coating of fiber tows. *Ceram. Eng. Sci. Proc.*, 1991, **12**, 1064–1074.
80. Cinibulk, M. K., Welch, J. R. and Hay, R. S., Preparation of thin sections of coated fibers for characterization by transmission electron microscopy. *J. Am. Ceram. Soc.*, 1996, **79**, 2481–2484.
81. Parthasarathy, T. A., Marshsall, D. B. and Kerans, R. J., Analysis of the effect of interfacial roughness on fiber debonding and sliding in brittle matrix composites. *Acta Metall. Mater.*, 1994, **42**, 3773–3784.
82. Kerans, R. J., Viability of oxide coatings in ceramic composites for accommodation of misfit stresses. *J. Am. Ceram. Soc.*, 1996, **79**, 1664–1668.
83. Parthasarthy, T. A. and Kearns, R. J., Predicted effects of interfacial roughness on the behaviour on the behaviour of selected ceramic composite. *J. Am. Ceram. Soc.*, 1997, **80**, 2043–2055.
84. Eriksson, G. and Pelton, A. D., Critical Evaluation of optimization of the thermodynamic properties and phase diagrams of the $CaO–Al_2O_3$, $Al_2O_3–SiO_2$, $CaO–Al_2O_3–SiO_2$ system. *Metall. Trans. B*, 1993, **24B**, 807–816.
85. Hallstedt, B., Assessment of the $CaO–Al_2O_3$ system. *J. Am. Ceram. Soc.*, 1990, **73**, 15–23.
86. Mizuno, M., Berjoan, R., Coutures, J. P. and Foex, M., Fig. 6438. System $Al_2O_3–La_2O_3$. In *Phase Diagrams for Ceramics*, Vol. VI, ed. R. S. Roth, J. R. Dennis and H. F. McMurdie. American Ceramic Society, Westerville, OH, 1987, p. 144.
87. Bondar, L. A. and Vinogradova, N. V., Fig. 2340. System $Al_2O_3–La_2O_3$. In *Phase Diagrams for Ceramics, 1969 Supplement*, ed. E. M. Robbins, C. R. Robbins and H. F. McMurdie. American Ceramic Society, Westerville, OH, 1969, p. 95.
88. Lewis, M., Cain, M., Doleman, P., Razzell, A. and Gent, J., Development of interfaces in oxide and silicate-matrix composites. *Ceram. Trans.*, 1995, **58**, 41–52.
89. Cain, M., Cain, R. and Lewis, M., In situ reacted rare-earth hexaaluminate interphases. *J. Am. Ceram. Soc.*, 1997, **80**, 1873–1876.
90. Longo, V. and Podda, L., Fig. 5437. System $ZrO_2–Al_2O_3–CeO_2$. In *Phase Diagrams for Ceramists*, Vol. IV, ed. R. S. Roth, T. Negas and L. P. Cook. American Ceramic Society, Westerville, OH, 1981, p. 228.
91. Mel'nik, M. T., Ved', E. I. and Ilyukha, N. G., Fig. 5367. System $BaO–ZrO_2–Al_2O_3$. In *Phase diagrams for ceramics*, Vol. IV, ed. R. S. Roth, T. Negas and L. P. Cook. American Ceramic Society, Westerville, OH, 1981, p. 197.
92. Bannister, M. J., Fig. 6686. System $CaO–Al_2O_3–ZrO_2$. In *Phase Diagram for Ceramists*, ed. R. S. Roth, J. R. Dennis and H. F. McMurdie. American Ceramic Society, Westerville, OH, 1987, pp. 304–305.
93. Cinibulk, M. K., Phase relations in the system lanthana–alumina–silica and reactions between lanthanum hexaluminate and mullite, unpublished.
94. Cinibulk, M. K., Reactions between hot-pressed calcium hexaluminate and silicon carbode in the presence of oxygen. *J. Am. Ceram. Soc.*, 1998, **81**, 2789–2798.
95. Parthasarathy, T. A., Mah, T. and Keller, K., Creep mechanism of polycrystalline yttrium aluminum garnet. *J. Am. Ceram. Soc.*, 1992, **75**, 1756–1759.
96. Corman, G. S., Creep of yttrium aluminum garnet single crystals. *J. Mater. Sci. Lett.*, 1993, **12**, 379–382.
97. Karato, S., Wang, Z. and Fujino, K., High-temperature creep of yttrium–aluminum garnet single crystals. *J. Mater. Sci.*, 1994, **29**, 6458–6462.